4th AIAA Atmospheric and Space Environments Conference
25 - 28 June 2012, New Orleans, Louisiana

AIAA 2012-2672

Aircraft Wake Vortex Decay in Ground Proximity - Physical Mechanisms and Artificial Enhancement

Anton Stephan* , Frank Holzäpfel † and Takashi Misaka ‡
Deutsches Zentrum für Luft- und Raumfahrt (DLR), 82234 Oberpfaffenhofen, Germany

Aircraft wake vortex evolution in ground proximity is investigated numerically with large eddy simulations (LES). The simulations are performed with different modifications of the ground surface in order to trigger rapid vortex decay or to simulate the landing of an aircraft. The impact of environmental turbulence in terms of turbulent winds is taken into account, where wall-resolved and wall-modeled LES are performed for low and high Reynolds number cases, respectively. In order to understand wake vortex decay mechanisms in ground proximity the interaction of primary and secondary vortices is thoroughly investigated. The results show that vortex decay is initiated and accelerated with obstacles at the ground. In order to optimize obstacle shape and size we show that we can achieve a similar effect with relatively small plates as with large block-shaped barriers. Concerning large Reynolds numbers we show that turbulence effects triggered by the ground can not be modeled by a simple wall model. As a first approximation of landing we use a ramp at the ground and show that the flow disturbances are similar to the result of flat ground with obstacles. In particular two kinds of so-called end effects are superposed: pressure waves in the vortex core and the propagation of the secondary vortex structures.

I. Introduction

As a consequence of lift generation by aircraft wings of limited span width, vortex sheets shed off the wings, roll up and form a pair of counter-rotating vortices. The evolving two-vortex system persists for a long period of time, possessing a high amount of kinetic energy and thereby posing a potential hazard to following aircraft. To avoid wake vortex encounters, regulatory separation distances between aircraft, dependent on their size, have to be met, which lead to a limit in the possible handling capacity of the airport. Therefore, the investigation of wake vortex decay is an important issue in commercial aviation.[1–3]

During the last decade, the evolution of wake vortices close to the ground has received much attention. In ground proximity the vortices can persist for a long period and still pose a hazard to following aircraft.[4–6] The evolution of a wake vortex system in ground proximity results in a complex three-dimensional flow. When counter-rotating vortices approach the ground or are generated at low altitudes, the proximity of a flat surface causes a divergence of the vortices. Induced by the vortices an outboard directed flow on the surface establishes and vorticity of opposite sign is produced in a boundary layer.[7] The induced flow near the surface experiences an adverse pressure gradient when passing the vortex cores, which is strong enough to cause a flow separation, leading to the formation of a separation bubble at the ground. Flow simulations show how pairs of secondary vortices are produced from the separation region.[8–10] They detach and interact with the primary vortices. The generated number of secondary vortices depends on the Reynolds number.[5] The presence of an ambient crosswind induces a boundary layer corresponding to a vorticity layer at the ground. In contrast to considerations without crosswind this causes an asymmetric situation. The sudden eruption of wake vortex induced wall vorticity is faster and more intense for the downwind vortex where the crosswind shear generated vorticity and the secondary vorticity have the same sign, but is attenuated for the upwind vortex. Researches during the last decades show that the decay of the wake vortex depends on a variety of parameters. There already have been numerous attempts to accelerate the decay deliberately out of ground.[11] However, much less work has been done for wake vortex decay acceleration in ground proximity.

*Graduate Student, Institut für Physik der Atmosphäre, Anton.Stephan@dlr.de
†Research Scientist, Institut für Physik der Atmosphäre
‡Research Scientist, Institut für Physik der Atmosphäre

The interaction of a counter-rotating two-vortex system with a flat surface using numerical simulations has been investigated so far with different approaches. Either wall-resolved direct numerical simulations (DNS),[12] or LES have been employed.[13] The resolution requirements for the boundary layer flow limit the Reynolds Number not only in DNS but also in LES. $\mathrm{Re}_\Gamma = \Gamma/\nu$ so far has been realized for Re_Γ around 20,000. Another possibility is to use wall-modeling functions,[14] which allows considering realistic Reynolds numbers up to 10^7. Similar as in Ref. 13 we mainly conducted wall-resolved LES at a Reynolds number of $\mathrm{Re}_\Gamma = 23,130$, though we discuss higher Reynolds numbers, too.

In this paper we analyse how boundary layer generated turbulence leads to wake vortex decay. With this knowledge we suggest a new method to accelerate vortex decay, based on fundamental properties of vortex dynamics. The vortex decay can be initiated locally and accelerated globally with dedicated obstacles installed at the ground. Roughly speaking the obstacle causes the flow to redirect the force that causes the wake vortices to rebound into turbulent vortex decay. We describe this effect qualitatively and determine how much wake vortex decay can be accelerated. It turns out that the design and arrangement of the obstacles can be optimized. So that this new method requires relatively small technical effort for testing and introduction at airports as it is ground-based and passive. In the latter part we model the landing process by the flight over a ramp. Also in this setup two kinds of disturbances appear that may be called end effects traveling along the primary vortices. One end effect is caused by an increase of pressure, propagating inside the vortex core, and another stems from the roll-up of secondary vorticity in the proximity of the ground.

In Sec. II we describe our numerical set-up. In Sec. III we present our results starting with an analysis of wake vortex decay mechanisms in the situation of a flat ground. Then we study the effect of one or two obstacles, and how this can enhance wake vortex decay. Later we examine different obstacle geometries in order to optimize them with respect to size and shape. Finally we approximate the final approach. In Sec. IV we summerize our results and draw conclusions.

II. Numerical Setup

A. Numerical Method

The LES is performed by using an incompressible Navier-Stokes code MGLET developed at Technische Universität München for solving the Navier-Stokes equations and the continuity equation[15]

$$\frac{\partial u_i}{\partial t} + \frac{\partial (u_i u_j)}{\partial x_j} = -\frac{1}{\rho_0}\frac{\partial p'}{\partial x_i} + (\nu_{\mathrm{mol}} + \nu_{\mathrm{turb}})\frac{\partial^2 u_i}{\partial x_j^2}, \tag{1}$$

$$\frac{\partial u_j}{\partial x_j} = 0\,. \tag{2}$$

Here u_i represents the velocity components in three spatial directions ($i = 1, 2,$ or 3), and $p' = p - p_0$ equals the deviation from the reference state p_0. Molecular viscosity ν_{mol} is set to $2.29 \cdot 10^{-2}$ $\mathrm{m}^2\,/\,\mathrm{s}$ and eddy viscosity ν_{turb} is obtained by a Lagrangian dynamic subgrid-scale model.[16] For density $\rho_0 = 1.2$ $\mathrm{kg}\,/\,\mathrm{m}^3$ is employed. Equations (1) and (2) are solved by a finite-volume approach with a fourth-order finite-volume compact scheme.[17] The simulations are performed in parallel using a domain decomposition approach.

B. Initial Vortex Pair

The fully rolled-up wake vortices are initialized by a pair of counter rotating Lamb-Oseen vortices with a circulation of $\Gamma_0 = 530\,\mathrm{m}^2\,/\,\mathrm{s}$, a vortex core radius of $r_c = 3.0\,\mathrm{m}$ and a vortex separation $b_0 = 47.1\,\mathrm{m}$, which are representative values for heavy aircraft. The Reynolds number is set to $\mathrm{Re}_\Gamma = \Gamma_0/\nu = 23,130$. The velocity scale is based on the initial descent velocity of the vortex pair $V_0 = \Gamma_0/2\pi b_0 = 1.79\,\mathrm{m}\,/\,\mathrm{s}$. This defines the non-dimensional time $t^* = t\frac{V_0}{b_0}$ with $t_0 = b_0/V_0 = 26.3\,\mathrm{s}$ and vorticity $\omega^* = t_0\omega$. For prescribing the initial vortex velocity field six image vortex pairs in spanwise direction and two mirror vortices in the direction perpendicular to the ground are taken into account.

C. Computational Domain

In our simulations we use two different domain sizes. The dimensions are either $L_x = 192\,\mathrm{m}$, $L_y = 384\,\mathrm{m}$, $L_z = 144\,\mathrm{m}$, see Fig. 1 or $L_x = 384\,\mathrm{m}$, $L_y = 288\,\mathrm{m}$, $L_z = 96\,\mathrm{m}$. This corresponds to approximately $4b_0 \times 8b_0 \times 3b_0$ or $8b_0 \times 6b_0 \times 2b_0$, respectively. The initial height of the vortex pair is set to $h_0 = b_0$ or $h_0 = b_0/2$. We impose periodic boundary conditions in the x and y directions. A no-slip condition is set at the ground at $z = 0$ and a slip condition at the top at $z = z_{\max}$. The number of grid points

are $N_x = 256, N_y = 512, N_z = 256$ or $N_x = 512, N_y = 384, N_z = 192$, respectively, leading to a total of 33.5 and 37.7 millions grid points. We employ a horizontally equidistant mesh. In vertical direction the mesh is stretched geometrically up to a height of b_0 and then is continued equidistantly until the top of the domain. We impose obstacles at the ground surface with square-shaped and rectangular cross section of $9\,\mathrm{m} \times 9\,\mathrm{m}$ or $9\,\mathrm{m} \times 4.5\,\mathrm{m}$. Obstacles at the ground surface are introduced in order to trigger the formation of secondary vortex structures (SVS) and to achieve premature vortex decay. They are modelled by introducing to the Navier-Stokes equations a drag force source term $F_{D,i} = C_D a|u|u_i$,[18] with constant drag coefficient $C_D = 0.1$ and a relatively high local matter density $a = 100\,\mathrm{m}^{-1}$ in the region of the obstacle.

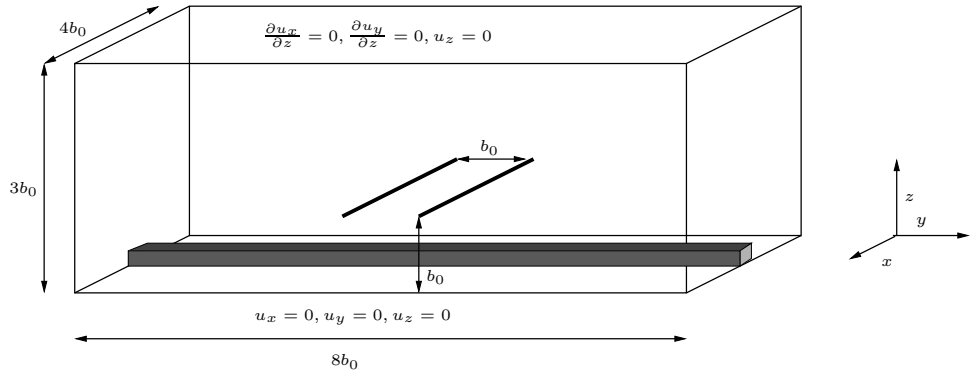

Figure 1. Schematic sketch of the computational domain showing the initial vortex position and an obstacle.

D. Ambient Wind

In order to provide a realistic environmental condition we establish a turbulent wind. This way we introduce time dependent velocity fluctuations modeling the atmosphere physically. The time-averaged stream-wise velocity of the wind at the initial vortex height is set to $0.85V_0$, where V_0 is the initial vortex descent velocity. A realistic wind situation consists of a three-dimensional turbulent flow, which is established in pre-simulations. Prescribing initially a vertical profile following the universal logarithmic law and imposing a stream-wise pressure gradient the wind flow is driven through the computational domain. In this setting the flow can be considered as a turbulent half-channel flow with the domain truncated in the middle of the channel, where a slip condition is applied. Here we shortly repeat basic properties of the channel-flow.[19]

Let δ denote the channel half height and consider the following quantities as averaged in time. For the boundary layer approximation the Navier-Stokes equations yield $\tau_w = -\delta \cdot \partial p/\partial x$, with constant pressure in wall-normal direction. The wall friction velocity is defined by $u_\tau = (\tau_w/\rho)^{1/2}$. This gives us the normalized values $u^+ = u/u_\tau$, $z^+ = zu_\tau/\nu$ and an intrinsic Reynolds number $\mathrm{Re}_\tau = u_\tau\delta/\nu$. The boundary layer of a turbulent flow has now three characteristic parts, the viscous sublayer, the transition layer and the logarithmic layer. In a fully developed flow each region has its own flow field characteristics. The viscous sublayer is shaped by coherent structures, so-called near-wall streaks . For Reynolds numbers $\mathrm{Re}_\tau < 1000$ this near-wall streaks are proven to have a spanwise spacing of $\lambda^+ \sim 100$.[20] To resolve the viscous sublayer wall-resolved LES requires a stretched mesh in wall-normal direction, with $z^+_{\min} < 1$. This limits our simulations to $Re_\tau = 530$ and $Re_\Gamma = 23,130$. To consider higher Reynolds numbers a wall model is needed. We employ a wall model based on the logarithmic law, to establish realistic velocity profiles, also known as the Grötzbach model.[21]

III. Results

A. Wake Vortex Evolution with Flat Ground

1. *Flow phenomenology*

In the early phase the approach of a vortex pair to a planar wall can be regarded as two dimensional. Early achievements in the framework of inviscid theory, which treat the boundary as free slipping, imply a monotonic descent of the vortices on hyperbolic trajectories.[22,23] However the viscous boundary layer changes the flow characteristics strongly.[19]

(a) $t^* = 1.3$ (b) $t^* = 1.8$

Figure 2. Wake vortex pair in crosswind situation. (a) Two levels of iso-surfaces $||w^*|| = 31.4$ and 3.14 as well as (b) iso-surfaces of $||w^*|| = 39.4$ colored by vorticity in span direction, ($h_0 = b_0$).

When the vortex pair descends it induces a vorticity layer at the ground, see Fig. 2.[7] An adverse pressure gradient builds up in the boundary layer while the primary vortices are diverging. The boundary layer bifurcates with a layer remaining close to the wall and a layer growing from the surface, which finally rolls up to secondary vortices and separates.[24] From numerical simulations, as well as field measurement campaigns[6] we observe a minimum descent height of about $b_0/2$, (assuming the vortices are initialized sufficiently aloft), up to the point, where secondary vortices detach.

Crosswind also induces vorticity close to the ground, which has opposite sign as the boundary vorticity layer of the up-wind vortex and the same sign to the vorticity layer of the downwind vortex, see Fig. 3. As a consequence vorticity layers generated by the wake vortices become unequally strong and the upwind and downwind vortices behave asymmetrically. The magnitude of the wake-vortex induced vorticity layer is growing leading eventually to separation and the generation of counter-rotating secondary vortices, first at the downwind and then at the upwind vortex. Then the secondary vortices rebound and interact with the primary vortices, which we will discuss later in detail. We also observe a roll-up process of the turbulent structures of the wind boundary layer while these disappear at the ground between the vortices, see Fig. 2 (a).

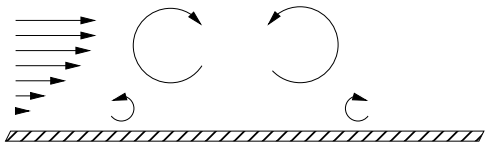

Figure 3. Sketch of wake vortex flow with crosswind.

2. *Trajectories and decay*

To know the exact position and the strength of the wake vortices is decisive for wake vortex prediction systems.[25] In the LES data primary and secondary vortex centers are tracked detecting local pressure minima and extreme values of vorticity. The axially averaged vortex core trajectories can be seen in Fig. 4 together with predictions of the deterministic and probabilistic two-phase wake vortex decay and transport model (D2P, P2P).[6,26] The averaged normalized closest distance to the ground of the primary vortices is 0.49 for the upwind and 0.57 for downwind vortex. Lidar measurements at Frankfurt airport indicate average altitudes of 0.525 and 0.62, respectively, in corresponding situations.[6] The measured lateral displacement of the primary vortex trajectories scatters around a median of 3.2 at average vortex ages of $t^* = 3$.[27] The LES provides exactly a lateral displacement of 3.2 at a time of $t^* = 3$. This good agreement indicates that the LES are representative for real wake vortex evolution in ground proximity.

One of main interest is the vortex strength that finally affects the aircraft. As a common measure of the vortex intensity for aircraft with a wingspan around 60 m we first consider $\Gamma_{5-15} = 0.1 \int_5^{15} \Gamma(r)dr$ for the primary and $\Gamma(5)$ for the secondary vortices, where $\Gamma(r) = \oint \vec{u} \cdot d\vec{s}$ denotes the circulation around a circle of radius r centered in the vortex core.[28] The evolution of these quantities is shown in Figure 5. In the early phase the circulation remains nearly constant. Then we have phase of rapid decay starting

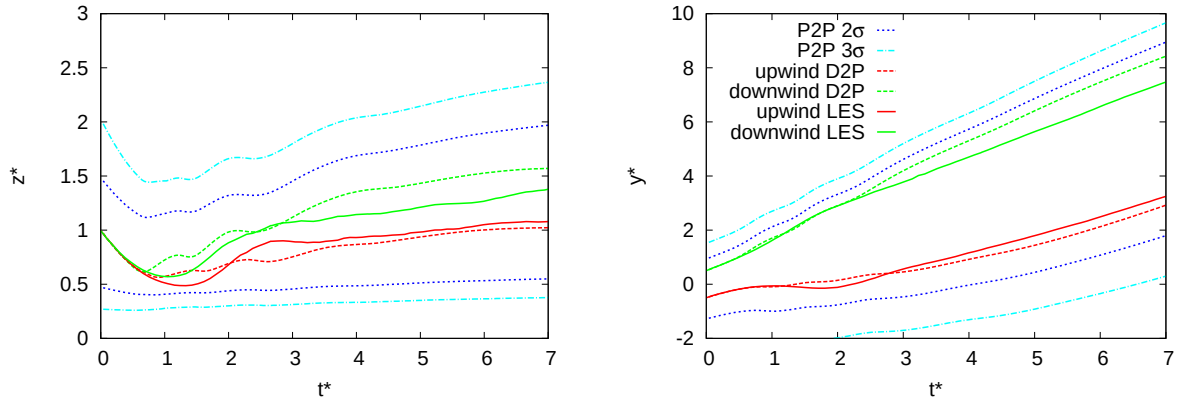

Figure 4. Evolution of normalized vertical and lateral vortex positions of wake vortices in crosswind situation. Results from LES (solid) compared with predictions from D2P and P2P wake vortex model.

for the upwind vortex at $t^* = 1.5$ and for the downwind vortex at 1.9 shortly after the secondary vortices have reached a maximum strength. Finally the circulation keeps decreasing slower, more pronounced for the downwind vortex again. It is worth mentioning that in spite of the rapid decay between $t^* = 1.5$ and 3 the core radius of the primary vortices is shrinking temporarily, see Fig. 5 (right).

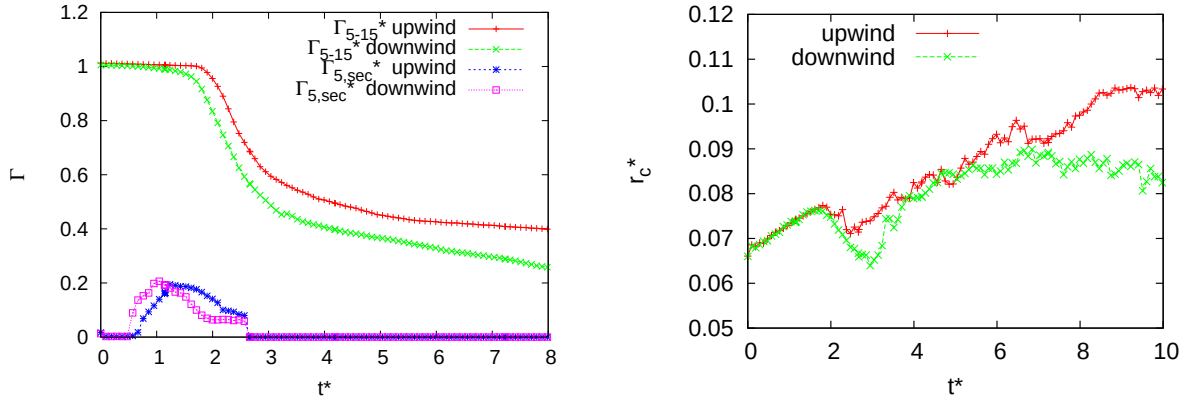

Figure 5. Evolution of vortex circulation for primary and secondary vortices (left) and core radius (right).

3. Wake vortex decay mechanism

In contrast to the wake vortex decay mechanisms that appear aloft, which are driven by atmospheric turbulence and thermal stratification,[29,30] the origin of turbulence here is the no slip condition at the ground, i.e. the strong shear established between the free crosswind flow and the zero velocity directly at the ground surface. The counter-rotating secondary vortices finally develop into relatively strong turbulent structures causing rapid decay. Figure 2 (b) shows that the secondary vortices do not detach as a whole from the ground but that hairpin vortices or omega-shaped vortices detach at distinct positions and then wrap around the primary vortices. As explained above this occurs first at the downwind and then at the upwind vortex. To our knowledge, the origin of this phenomenon is not well documented and explained so far. First we focus on the origin of these instabilities in our simulations.

A closer look at the velocity distribution at the ground, before imposing the vortex system reveals a wave-shaped pattern of highly elongated structures, the so-called streaks seen in Fig. 6 (left).[20] These streaks correspond to regions of high velocities oriented in span direction (u_y) in immediate ground proximity. Regions of high crosswind velocity (gradients) and low crosswind velocity (gradients) at the ground strengthen or weaken the roll-up process of the secondary vortices, respectively, see Fig. 3. So a region of small vertical wind gradients at the upwind secondary vortex and a region of high wind gradients at the downwind secondary vortex both enforce the secondary vortices to detach earlier, as shown in Fig. 6. The shape and development of the omega loops are clearly visible in Fig. 6 (left) below at the downwind vortex, whereas the correlation of the boundary layer streaks and the omega loops is even more obvious for the upwind vortex, see Fig. 6 (right).

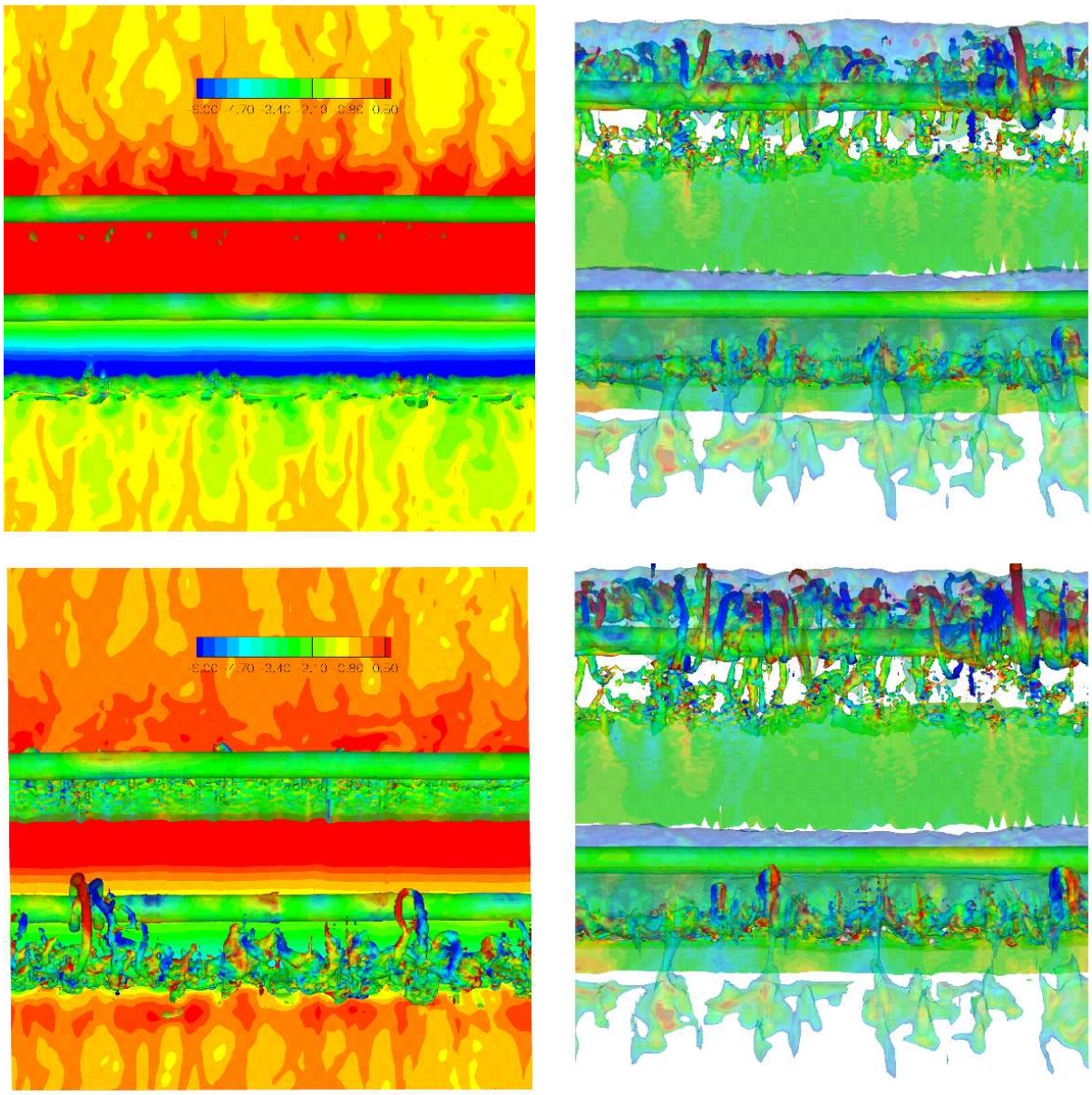

Figure 6. Velocity irregularities at the ground trigger hairpin vortices. Iso-surface of vorticity magnitude $||w^*|| = 39.4$ combined with (left) velocity at the ground at $t^* = 0.95$ (top) and 1.52 (bottom) and (right) with iso-surface of velocity $v* = 0.06$ (translucent) at $t^* = 1.61$ (top) and 1.71 (bottom); the lower vortex is the downwind (left) and the upwind (right) vortex, ($h_0 = b_0$).

As a consequence we may expect a correlation of the streak spacing of the crosswind flow and the spacing of secondary vortex disturbances. The streak spacing has found to be $\lambda^+ = 100$ in experiments[31] as well as in numerical simulations for relatively small Reynolds numbers.[20] Ref. 32 gives evidence that $\lambda^+ = 100$ also holds for high Reynolds numbers. Consequently, the wave length of the secondary vortices is highly dependent on the Reynolds number. The following bullets provide a first description of wake vortex decay in ground proximity in five steps.

- The formation of secondary vortices is favored at crosswind velocity excess or deficit for the lee and luv vortex, respectively, triggered by instabilities like crosswind streaks
- The subsequent stretching and tilting of the secondary vortices by the primary vortex causes intense omega loops (hairpin vortices)
- Omega shape causes a self-induced fast approach to the primary vortex
- After the secondary vortex has looped around the primary vortex, the omega head widens driven by self induction
- The interaction of approaching secondary vortices and primary vortex causes turbulence and annihilation of vorticity

The prominent role of secondary vorticity structures for wake vortex decay is well known and has been analyzed in detail in Ref. 30. The formation of omega loops from secondary vortices has been studied in Ref. 33. We will have a closer look at these mechanisms when we investigate the effect of obstacles at the ground.

B. High Reynolds Number Flows

In a simulation with $\mathrm{Re}_\Gamma = 231,300$ and $\nu = 2.29 \cdot 10^{-3}\,\mathrm{m}^2\,/\,\mathrm{s}$ we investigate how the Reynolds number affects vortex decay. We impose a wall model based on the logarithmic wall law, to achieve the characteristic boundary layer velocity profile in the pre-simulation. Again we use a pressure driven flow with the same pressure gradient $dp/dy = 5.9 \cdot 10^{-5}\,\mathrm{N}\,/\,\mathrm{m}^3$ as before. As expected the spacing between the detaching SVS become much smaller. The SVS are actually not well resolved anymore, see Fig. 7 (left). The vortex decay at the 10 times larger Re number appears to follow the same physics but is somewhat

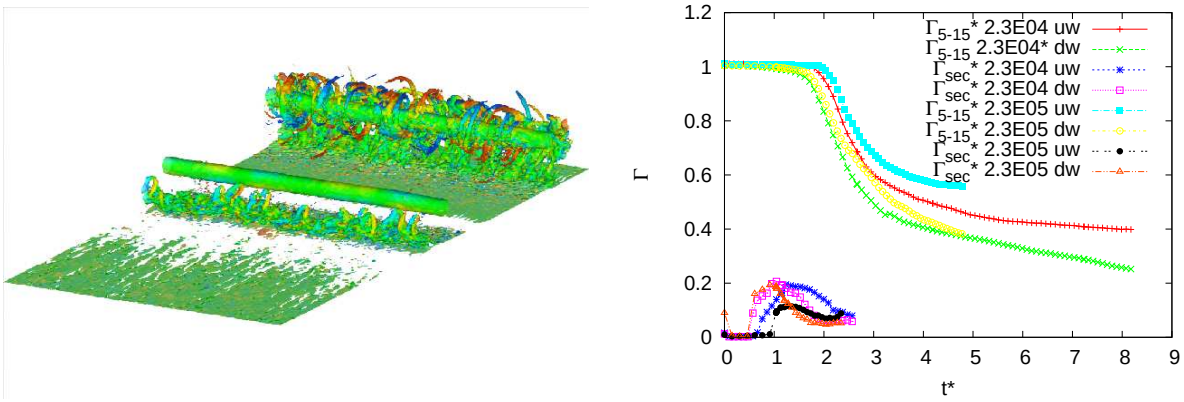

Figure 7. Iso-surface of vorticity magnitude $||w^*|| = 39.4$, colored by vorticity in span direction, at $t^* = 1.66$ (left), evolution of vortex circulation for primary and secondary vortices for different values of Re (right), ($h_0 = b_0$).

delayed and the circulation after decay is slightly higher than in the low Reynolds number case, see Fig. 7 (right). This supports the idea from the last sections that turbulence generated from the ground, i.e. excesses and deficits in the boundary layer velocity, lead to wake vortex decay. As any wall model will lack to reproduce fine coherent structures at the ground, we may not expect correct results by using wall models. To achieve realistic vortex decay, we might need wall-resolved LES also for high Reynolds number cases.

Certainly, it is of interest what kind of instabilities will occur in the viscous boundary layer at large Reynolds numbers at real airports. Having in mind that the streak spacing scales approximately with the molecular viscosity we see that these will not be crucial for realistic viscosities. Instead always present surface irregularities such as tussocks will influence the boundary layer flow and thus the SVS on

larger scales. We assume that instabilities caused by streaks in our previous simulations ($\mathrm{Re} = 23,130$) represent irregularities from the airport terrain well. So our simulations might give a good approximation of wake vortex behavior at real airports.

C. Obstacle effect

1. Flow field

In this section we compare wake vortex flows above flat ground with flow above ground with obstacles under the influence of a crosswind. When we impose an obstacle at the ground surface the flow changes substantially. At the top of the barrier secondary vorticity is generated rapidly after vortex initialization, which subsequently detaches and develops a distinct loop, see Fig. 8 (right). The loop is stretched and winds around the primary vortex forming an omega-shaped loop, approaching and immersing into the primary vortex. The process follows the vortex stretching and tilting mechanisms explained in Ref. 30. The geometrically induced SVS travel along the primary vortices driven by self-induced velocity induction while they weaken the primary vortices efficiently as we will investigate in detail. In Fig. 8 (left) we see that for flat terrain the separation process just begins at a time of $t^* = 1.35$ whereas with the obstacle already substantial disturbances engulf the primary vortices, see Fig. 8 (right).

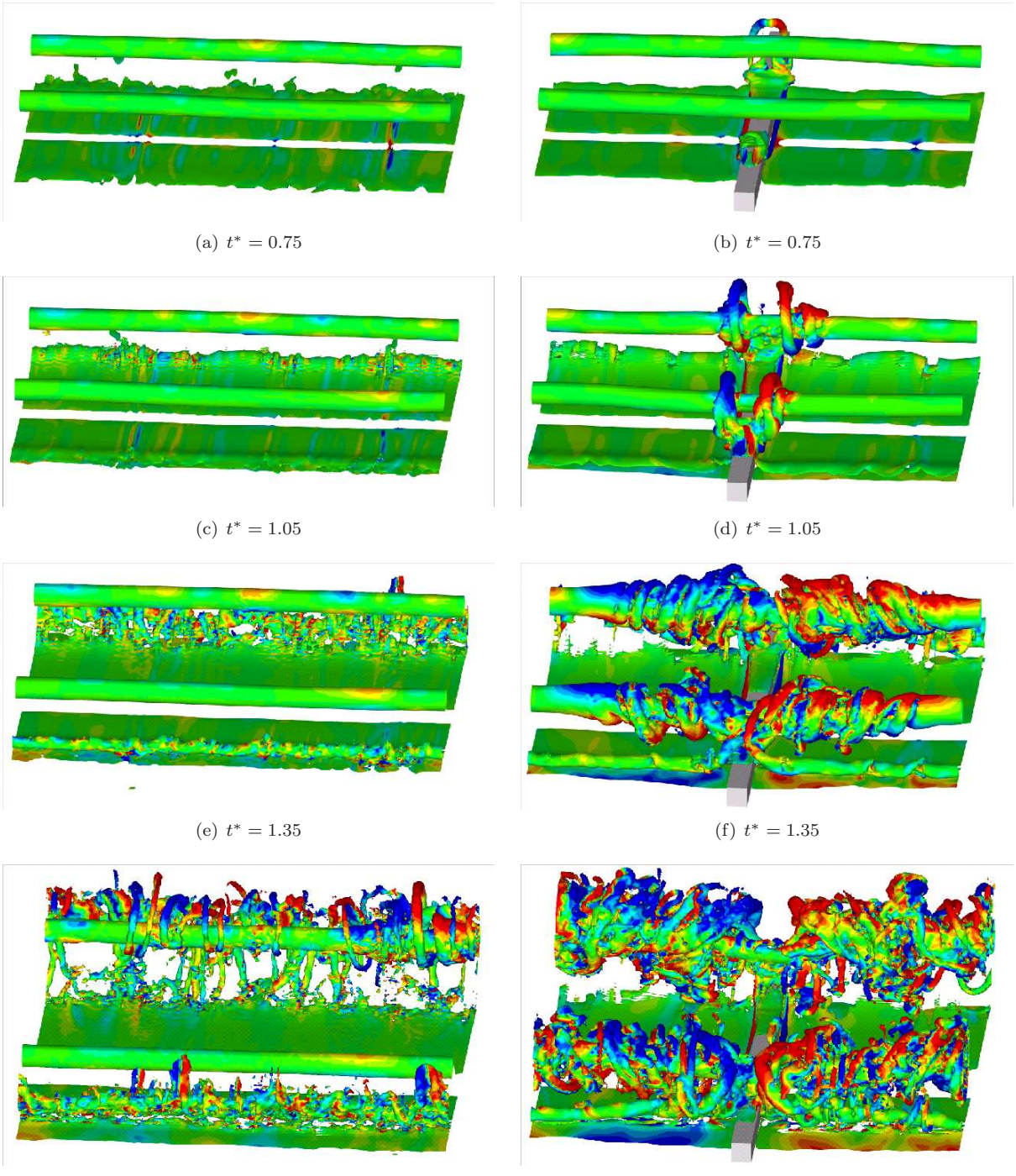

(a) $t^* = 0.75$ (b) $t^* = 0.75$

(c) $t^* = 1.05$ (d) $t^* = 1.05$

(e) $t^* = 1.35$ (f) $t^* = 1.35$

(g) $t^* = 1.75$ (h) $t^* = 1.75$

Figure 8. Wake vortex evolution with crosswind without (left) and with obstacle (right) at the ground. Iso-surfaces of $||w^*|| = 39.4$ colored by vorticity in span direction, ($h_0 = b_0$).

2. *Trajectories and Decay*

Now we analyse the enhanced decay characteristics quantitatively. Furthermore we are interested in the change of trajectories, i.e. whether rebound height is influenced by an obstacle or not. We have to keep in mind that we use periodic boundary conditions. So interpreting the simulations correctly, we do not calculate the influence of one obstacle, but periodically arranged obstacles with a separation equal to the domain length of $4b_0$. However, until the disturbance reaches the domain boundary we can neglect the influence of other obstacles. Because of the intense interaction of primary and secondary vortices it becomes very difficult to track the vortices, especially the downwind vortex, for larger times than $t^* = 3$.

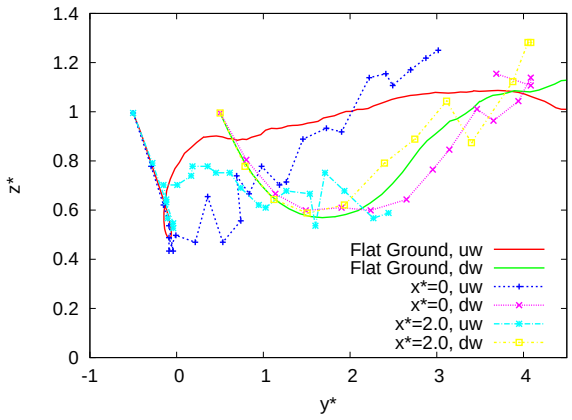

Figure 9. Vortex center trajectories, for flat ground and different distances from an obstacle with $0.2b_0 \times 0.2b_0$ cross section. The series of points starts at $t^* = 0$ and proceeds with steps of 0.3.

Lateral advection of the primary vortices plays an important role for the clearance of the flight corridor during final approach. Due to the weak crosswind the upwind vortex may hover above the runway for a long time, as depicted in Fig. 9. This is a potentially hazardous situation for following aircraft. We see that an obstacle does not change that fact. Figure 9 shows the results of wake vortices initialized at b_0. The primary vortices can rebound to a height of about $1.1b_0$ above flat ground. Directly above the obstacle the rebound height is much reduced but can exceed the height above flat ground at later times when circulation is already much reduced, see Fig. 10. In a distance of $x^* = 2.0$ the rebound remains consistently below that with flat ground.

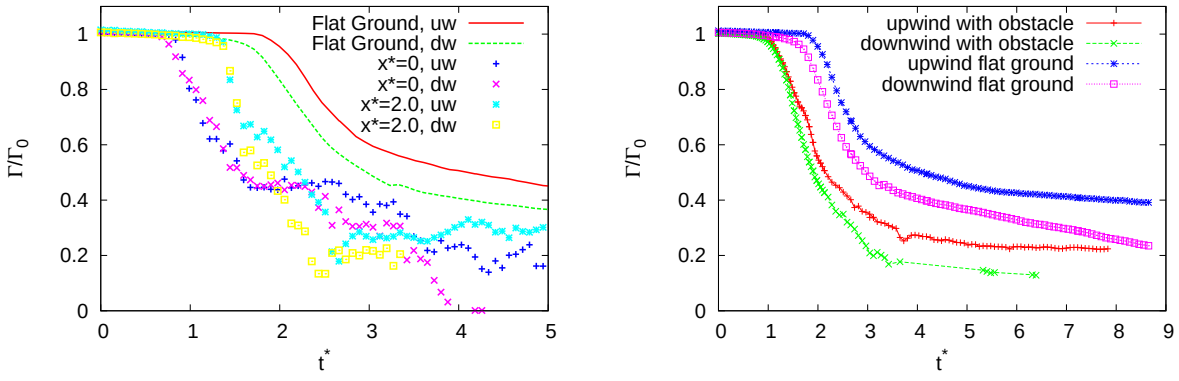

(a) (b)

Figure 10. Vortex circulation Γ_{5-15} in crosswind situation, flat ground and obstacle with $0.2b_0 \times 0.2b_0$ cross section, (a) different distances from the obstacle (b) averaged in axial direction.

Above the obstacle we observe a tremendous and rapid reduction of the circulation to 40% of the initial circulation, see Fig. 10 (a), whereas in case of flat ground the circulation does not change significantly. We further observe that in a distance of $2b_0$ from the obstacle the circulation is also reduced faster. Although the decay does not develop uniformly along the vortex we average Γ_{5-15} in axial directions for comparison with the flat ground. During the initial descent the vortex strength remains nearly constant for one t_0 in case of an initial vortex height of $h = b_0$, see Fig. 9 (b). The decay starts when secondary

vorticity immerses in the primary vortices. With crosswind vortex decay proceeds asymmetrically. The downwind vortex decays faster and reaches lower values than the upwind vortex. As we can see in Fig. 9 (b), the obstacle reduces Γ_{5-15} to a half compared to the case without obstacle after a time of $2t_0$.

3. Detailed analysis of vortex dynamics with obstacle

As we could see, the main reason for vortex decay in flows with obstacles is the obstacle itself that causes a strong instability of the SVS. So for clarity we will investigate the vortex dynamics without the influence of crosswind. However in that case no reasonable comparison with the flat ground can be made because vortices above flat ground and no source of turbulence like crosswind behave laminar for a long time.

We suggest that the following five characteristics of the phenomenon redirect a substantial part of the force that normally causes the wake vortices to rebound into premature vortex decay.

1. Early detachment of strong omega-shaped secondary vortices

Depending on the obstacle height secondary vorticity detaches earlier. Because the distance to the primary vortices is smaller than $b_0/2$ the strength of these SVS is also increased, see Fig. 8. In our simulations we found a secondary vortex strength of up to one third of the primary vortices.

2. Omega shape causes self-induced fast approach to the primary vortex

Once the secondary vortices become irregular due to the obstacle (or other instabilities) the flow can no longer be considered as two dimensional. The early detachment of the vorticity layer above the obstacle leads to a omega-shaped SVS. In Fig. 11 we see the early phase after the disturbance by the obstacle. First (left) we observe how the hairpin vortex induces a velocity towards the primary vortex, which speeds up the interaction between the vortices. Simultaneously the omega-shaped SVS is stretched around the primary vortex in its velocity field as detailed in Ref. 30. The omega-shaped SVS induces a velocity in the direction of the primary vortex core, see Fig. 11 (left). Subsequently the spirally moving secondary vortex induces itself a streamwise velocity similar to vortex rings, as shown in Fig. 11 (right).

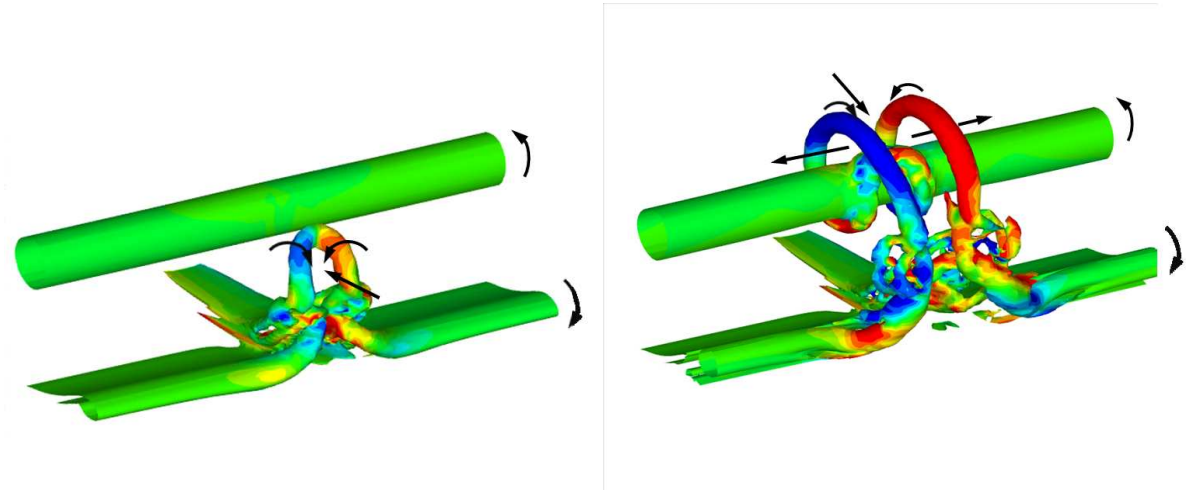

Figure 11. Omega-shaped SVS detaches from the obstacle and induces a velocity towards the primary vortex (left), rolled-up SVS induces streamwise propagation velocity (right).

3. After the secondary vortex has looped around the primary vortex it travels along the primary vortex again driven by self induction

The helically looped vortex travels streamwise up and down the primary vortex and merges with its vortex core, see Fig. 8. The secondary vortex takes the shape of a screw. As the looped secondary vortex reverses its orientation, see Fig. 12 (a), the vorticity has the same sign as the vorticity of the primary vortex. The primary vortex is deformed by the secondary vortex, resulting also in a helical structure of the primary vortex. A double helix is created, becoming larger and larger, see Fig. 12 (a). Here we observe two complementary effects, leading to an axial velocity inside the vortex, see Fig. 12 (b).

(i) When the flow takes the form of a double helix, primary and secondary vortices have the same sense of rotation and helicity and consequently induce an axial velocity to the same side inside the double helix, see Fig. 12 (b).
(ii) We also observe axial velocity in the vortex core in regions far ahead of the helix, see Fig. 12 (b). The second effect is due a reduction of the circulation above the obstacle, see Fig. 13 that locally increases the pressure in the vortex core. This corresponds to a pressure gradient inside the vortex core in axial directions, which induces axial velocities in the core, see Fig. 13. The pressure wave starts at a time of $t^* = 0.08$ and reaches the boundary at a time of $t^* = 0.53$, corresponding to a propagation speed of $U_p^* = 8.8$. Propagation of pressure waves in Lamb-Oseen vortices has been thoroughly investigated in Ref. 34.

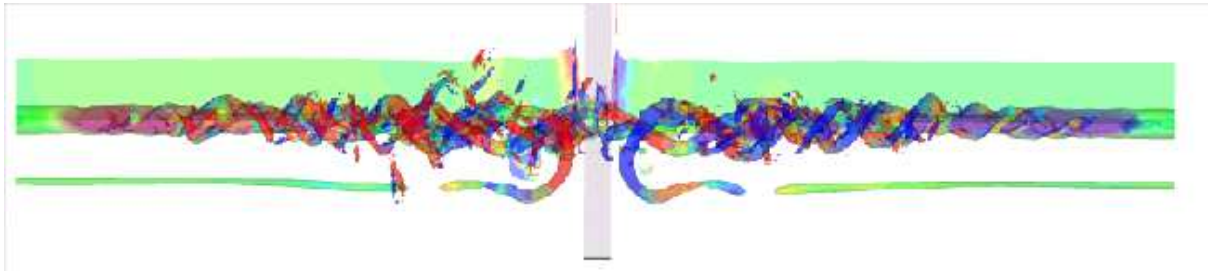

(a)

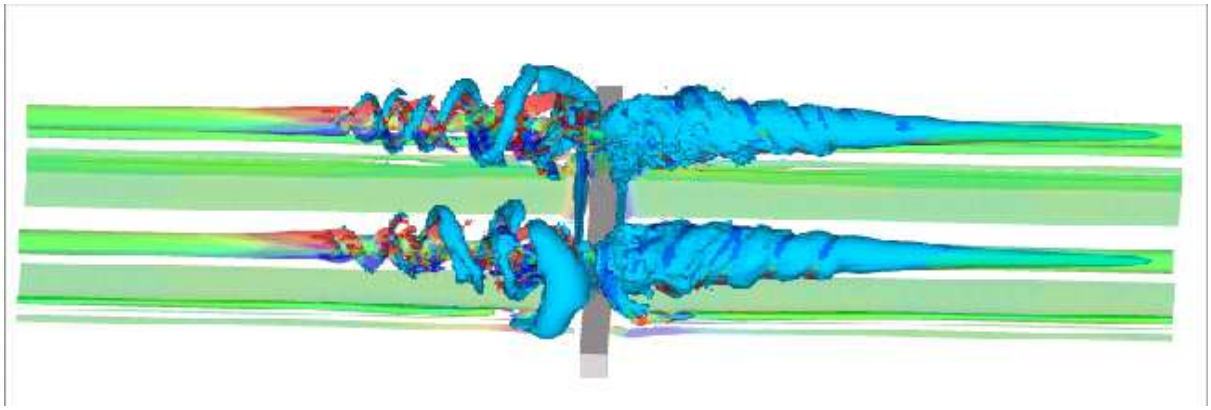

(b)

Figure 12. Iso-surface of vorticity magnitude colored with vorticity in flight direction, (a) forming a double helix at $t^* = 0.84$,(b) with an iso-surface of axial velocity $u_x^* = 0.56$ at $t^* = 0.61$, ($h_0 = b_0/2$).

The spiral disturbance can be approximated as a ring at least in the first stage of its roll-up. As already mentioned vortex rings move with a self-induced velocity that depends on ring radius R, the core radius a and the circulation Γ of the ring vortex. If we neglect the viscosity, the induced ring speed of a thin vortex ring can be computed with the following formula:[22]

$$U = \frac{\Gamma}{4\pi R}\left(\log\frac{8R}{a} - 0.25\right). \tag{3}$$

We consider the positions of the first and the second maximum of the helix, see e.g. Fig. 12 (b), estimating a core radius of 0.02 and 0.04 respectively, see Fig. 14 (left). We evaluate the circulation and ring radius of the secondary vortex at different points to compute the propagation speed according to Eq. (3), see Fig. 14 (right). Apparently Eq. (3) underestimates the propagation speed. In particular in the later stage the helical and tapered shape seems to behave differently compared to a simple vortex ring.

4. The dedicated secondary vortex connects to the regular ground effect vortex and thus obtains continued supply of energy

As we can see in Fig. 11 the secondary vortex detaches much faster above the obstacle. However it stays connected in accordance to Helmholtz laws, although the shape of the obstacle is not smooth. Iso-surfaces of vorticity magnitude in Fig 12 show the connected secondary vortex until the flow is getting turbulent.

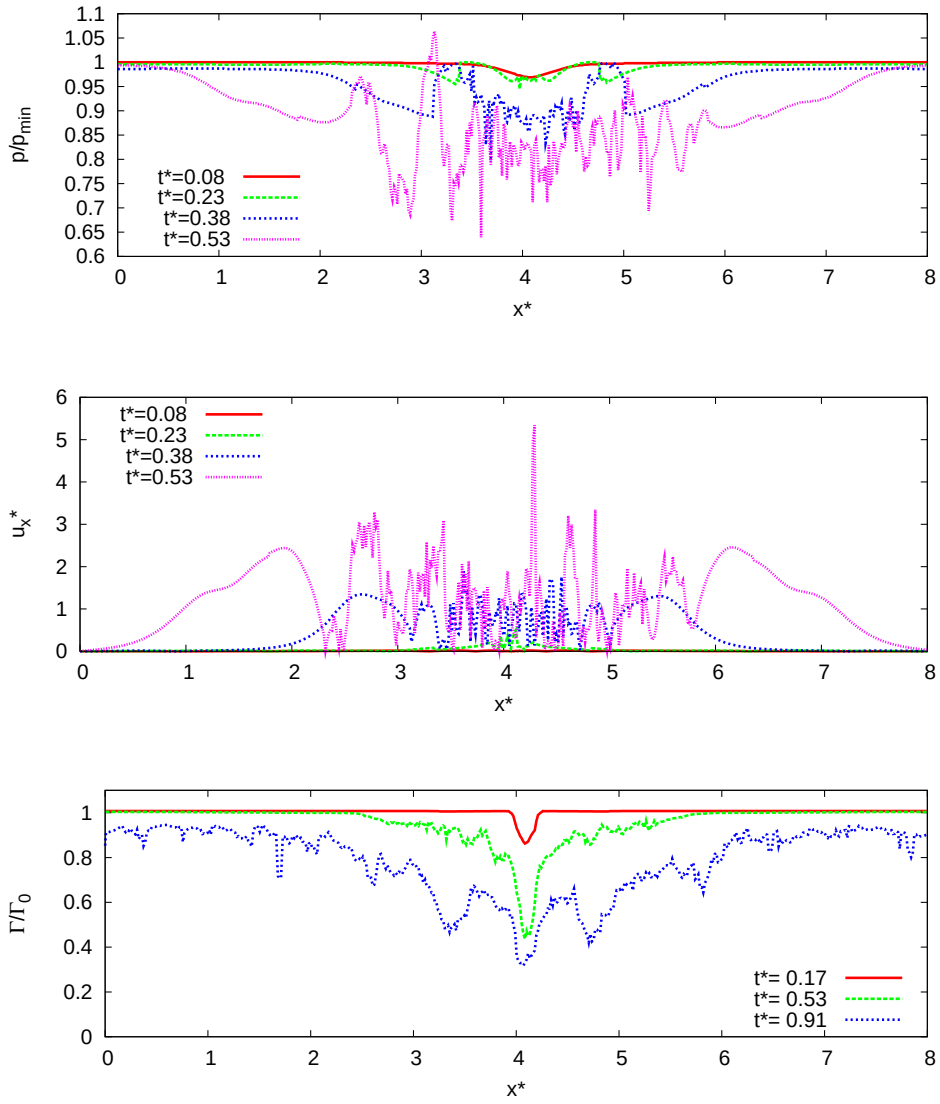

Figure 13. Distribution of $p/p_{\min}, u_x^*$ along the vortex center and Γ_{5-15} at different times, ($h_0 = b_0$).

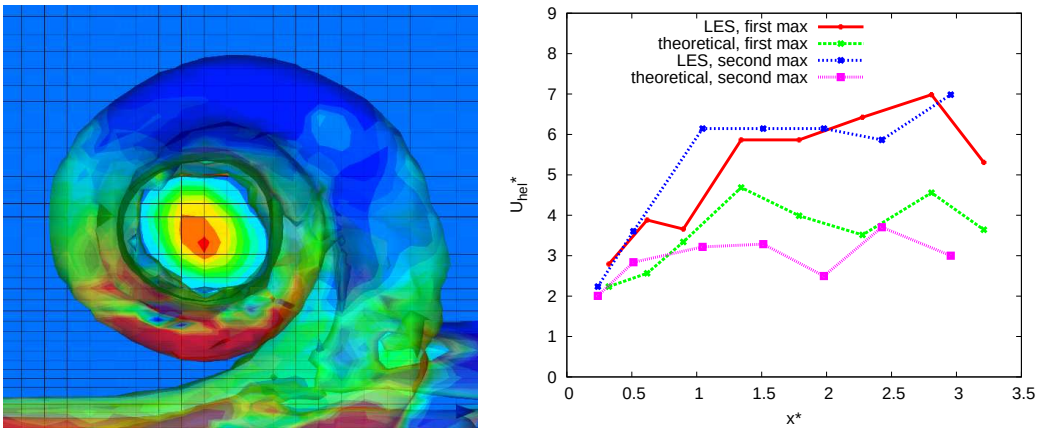

(a) Cross section vortex spiral

(b) Ring speed development

Figure 14. (a) Estimation of core radius. Iso-surfaces of $||w^*|| = 39.4$ (translucent) and plane parallel to vortex, horizontal grid spacing $\Delta y^* = 0.03$. (b) Propagation speed of first and second helix maximum compared with theoretical speed of a ring.

5. The highly intense interaction of primary and secondary vortices

The decay rates of the wake vortices highly depend on the interaction with the turbulent environment.[30] The circulation reduces while the primary vortex is conducting work on turbulent structures and mixes with these. The stronger the turbulent structures the faster the vortex decay. SVS, as strong environmental structures in ground vicinity, trigger the vortex decay close to ground. Obstacles lead to an earlier interaction of higher intensity than the flat ground, which was quantified in Sec. C.2. With obstacles the five listed flow characteristics lead to rapid wake vortex decay independent from natural external disturbances.

D. Effect of Several Obstacles

Considering a wake vortex ground approach with several axially displaced obstacles leads to the question how the previously discussed disturbances interact. Assuming sufficiently large separations of the obstacles we have no interaction of the omega-loops at the first stage of the flow but after the roll up process and propagation along the primary vortices. Now we investigate what happens when disturbances coming from two obstacles collide.

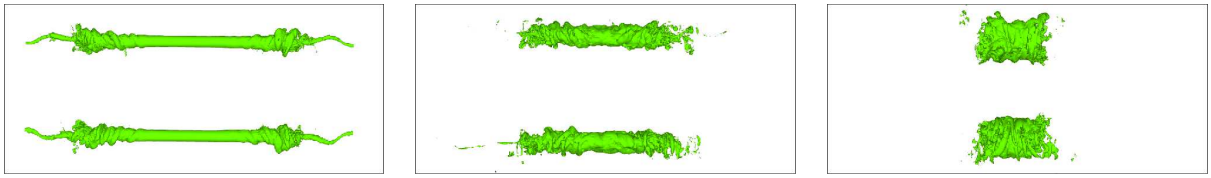

(a) $t^* = 0.76$ (b) $t^* = 1.14$ (c) $t^* = 1.52$

Figure 15. Distribution of passive tracer in case of two obstacles. ($h_0 = b_0/2$)

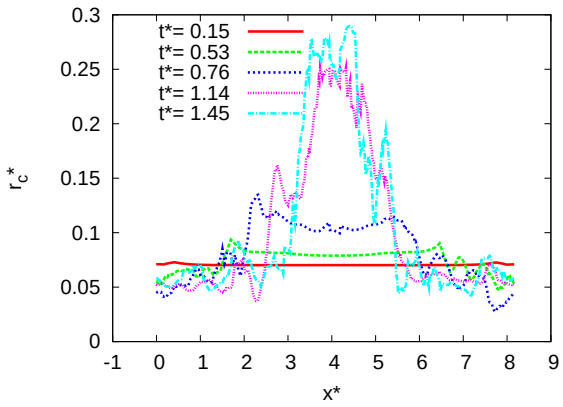

Figure 16. Vortex core radius along the vortex center line derived from LES for different time steps.($h_0 = b_0/2$)

In our simulations we assume fully rolled-up vortices approaching the obstacles at the same time. Consequently we have a symmetric situation. The collapse of the propagating disturbances occurs exactly in the center between two obstacles. In reality the second obstacle will influence the wake vortex with an offset in time due to the flight speed and flight path angle. As a consequence the collapsing point of the disturbances will be shifted axially.

As mentioned we use our above described simulations with periodic boundaries. For visualization we just cut one half of the domain and connect it from the other side to the other half, see Fig. 15. We see colliding disturbances coming from two obstacles and an accumulation of fluid marked by a passive tracer initialized in the vortex core. Eventually the vortex bursts. Similar effects are discussed thoroughly in Ref. 29.

Figure 16 shows the development of the core radius. We see a rapid increase of core radius after the disturbance has reached the boundary, i.e. after the collision.

E. Effect of Different Obstacle Geometries and Headwind

In this section we discuss the shape and the size of the obstacles. In our setting we use 0.2×0.2 square profiles in normalized coordinates, which corresponds to a barrier of $9\,\mathrm{m} \times 9\,\mathrm{m}$ square cross section in reality. This appears quite high for realistic applications at airports. In this section we reduce the obstacle height to $h^* = 0.1$ keeping the width fixed. Moreover a two dimensional geometry requires a lot of material and might conflict with escape routes of departing aircraft. Here we investigate whether we can reduce the obstacle height and volume without reducing the favorable effects on wake vortex decay. The idea is to mimic the block shape with thin plates at intervals of $\Delta y^* = 0.45$ (21m) to achieve a similar effect. So far we did not care about headwind that leads to an axial transport of the primary and secondary vortices across the obstacles. In the boundary layer the headwind has relatively strong gradients in wall normal direction. In this section we also investigate the influence of a headwind on the roll-up of SVS and primary vortex decay.

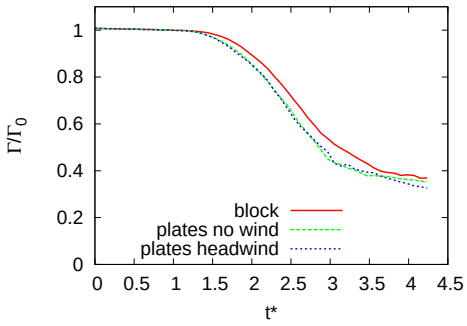

Figure 17. Evolution of Γ_{5-15} averaged in flight direction for different geometries and wind configurations.

From Fig. 17 (left) we observe that flat plates arranged consecutively lead to a similar effect like a block-shaped obstacle. SVS separate nearly at the same time, although the contours are a bit less defined, see Fig. 18. The headwind shifts the rolled-up SVS, however every one of the listed effects, which we described in Sec. C.3, can be observed.

The decay above the flat plates starts slightly earlier, see Figs. 17, 18. Apart from that the characteristic circulation distributions lock very similar in case of no wind. Although the headwind shifts the roll-up of the SVS the effect of the plates appears to be very robust and the averaged circulation decay is not influenced, see Fig. 17.

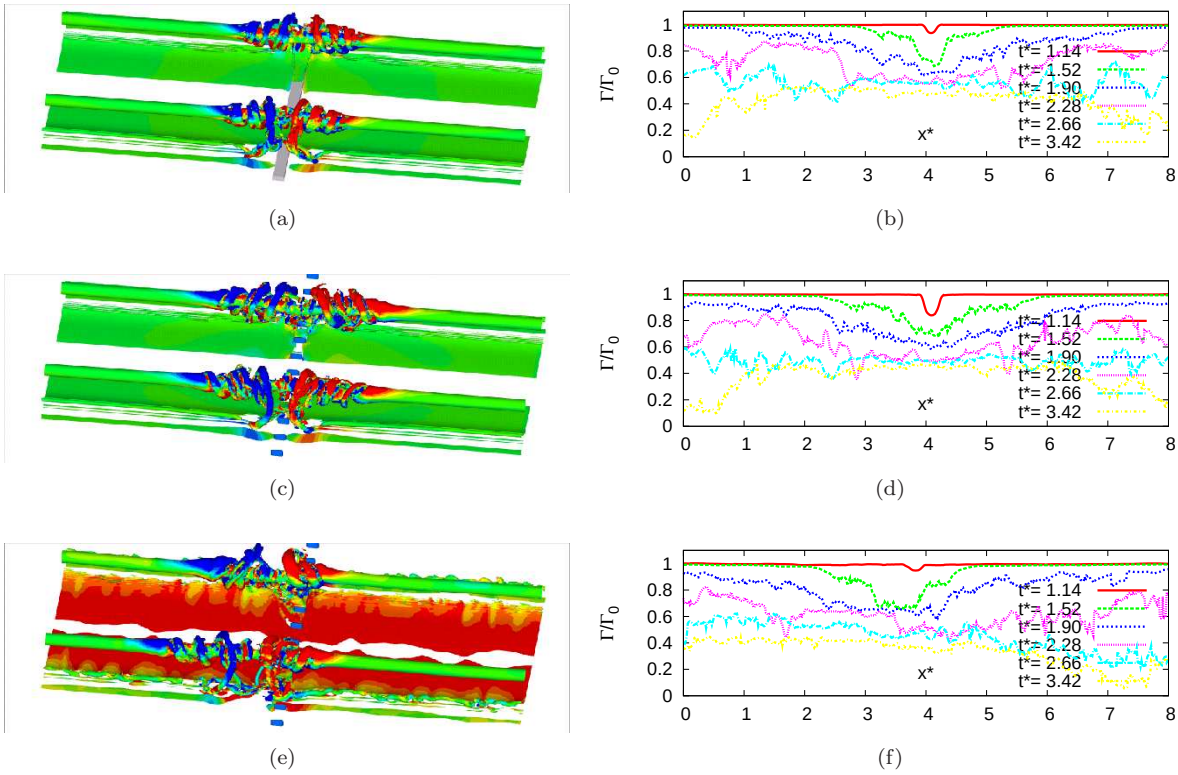

Figure 18. (left) Iso-surfaces of $||w^*|| = 52.6$ colored by vorticity in span direction at a time of $t^* = 1.52$, (right) distribution of Γ_{5-15} at different times, (a), (b) block-shaped obstacle (c), (d) flat plates (e), (f) flat plates with headwind from right to left, ($h_0 = b_0$).

F. Simulation of Landing

When simulating the final landing approach with LES we face two serious technical problems. First the lift of the aircraft strongly reduces during the touch-down. This leads to a circulation reduction of the wake vortices. Consequently we cannot initialize the wake vortex equally along the center line. Another problem is that we have to initialize vortices along the descending flight path of three degrees in our simulations, where we cannot use periodic boundary conditions in flight direction. The second problem can be overcome by transforming the coordinates such that the airplane does not descend but remains at a certain height above the ground. Conversely the ground has to be tilted. If we mirror the ramp and initialize fully rolled-up vortices we can circumvent the second problem and consider this setting as a first simple approximation of a real landing process, see Fig. 19.

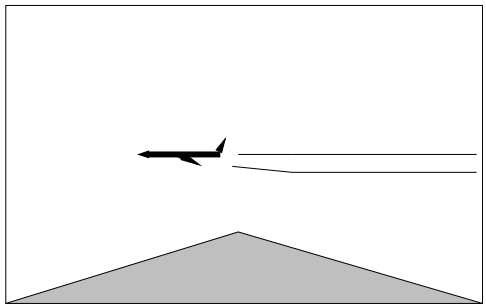

Figure 19. Computational setting for simulating wake vortices with landing angle to the ground.

Qualitative results as well as properties of the flow field can be obtained with this setup. In reality there will appear so called end-effects due to circulation reduction at the touch-down, which we will not be able to observe. But the interaction of the inclined vortices with the ground will be visible in our setting.

Figure 20 reveals that a ramp has a similar impact on the flow as an obstacle. The main difference is the linear variation of the vortex height above ground, which leads to inclined secondary vortices. The smaller the distance between primary and secondary vortices the faster their interaction. SVS separate earlier at the top and wind around the primary vortices, see Fig. 20 (left). Again we observe the five characteristic steps from Sec. C.3. Two kinds of end effects are propagating along the primary vortex, as explained in step 3. One coming from a pressure increase traveling inside the vortex core, see Fig. 20 (right) and one coming from helically rolled-up SVS outside the vortex core, traveling approximately half as fast.

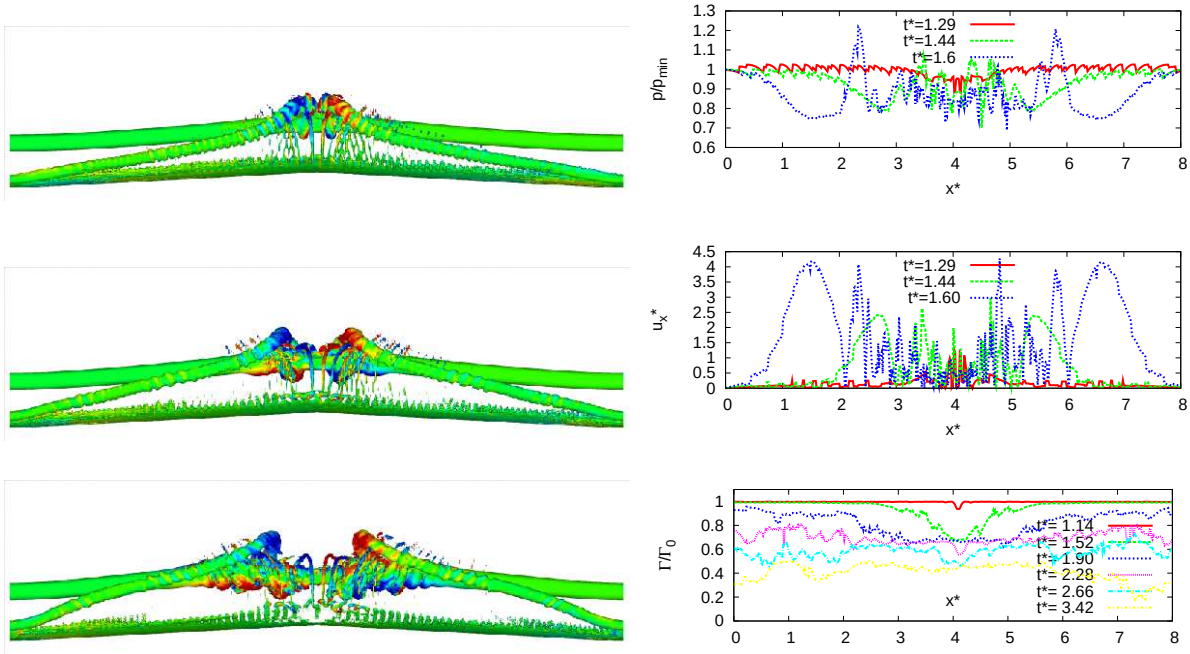

Figure 20. (left) Iso-surfaces of $||w^*|| = 35.5$ colored by vorticity in span direction at times $t^* = 1.29$, $t^* = 1.44$ and $t^* = 1.6$. (right) Distribution of p, u_x^* and Γ_{5-15} at different times. ($h_0 = b_0$)

IV. Conclusion

We conduct several wall-resolved LES to study wake vortex in ground effect with and without crosswind. A simple wall model was also tested. The investigation of the decay mechanisms reveals that instabilities of the secondary vortex structures trigger rapid vortex decay of the primary vortices. In order to further accelerate vortex decay in ground proximity we impose obstacles different in type and shape. This setup allows the dedicated use of properties of vortex dynamics to accelerate wake vortex decay in ground proximity with the following characteristics:

- Early detachment of strong omega-shaped secondary vortices
- Omega shape causes self-induced fast approach of the primary vortex
- After the secondary vortex has looped around the primary vortex it separates and travels along the primary vortex again driven by self induction
- The dedicated secondary vortex connects to the regular ground effect vortex and thus obtains continued supply of energy
- The highly intense interaction of primary and secondary vortices leads to rapid wake vortex decay independent from natural external disturbances

Disturbances caused by two barriers collide midway between the barriers leading to vortex bursting. The obstacles are optimized with respect to size and shape. We could show that a plate line causes an even slightly stronger effect than a much more massive block-shaped barrierer. Headwind does not degrade the averaged circulation decay triggered by the plate line. Finally the landing approach is simulated using a ramp with an approach angle of three degrees. Here similar effects like in the flow above an obstacle is observed. We identify two kind of end effects. One stemming from a pressure wave inside the vortex core and one coming from propagating helical vortex structures that develop from the rolled-up secondary vortices.

In summary the introduction of obstacles at the ground supports the selective generation of secondary vortices and smart utilization of vortex properties in order to generate fast approaching and rapid spreading of disturbances along the primary vortex leading to premature vortex decay in ground proximity. The installation of suitable obstacles at runway tails may improve safety by reducing the number of wake encounters and increase the efficiency of wake vortex advisory systems. A respective patent has been filed under number 10 2011 010 147.

Acknowledgments

The simulations have been performed using supercomputers at Deutsches Klimarechenzentrum (DKRZ), Forschungszentrum Jülich and Leibniz-Rechenzentrum (LRZ). We would like to thank Dr. Andreas Dörnbrack for providing computation time at DKRZ as well as Prof. Dr. M. Manhart for providing the original version of the LES code MGLET. The work was funded by DLR project Wetter & Fliegen.

References

[1]Gerz, T., Holzäpfel, F., and Darracq, D., "Commercial aircraft wake vortices," *Progress in Aerospace Sciences*, Vol. 38, No. 3, 2002, pp. 181–208.

[2]Gerz, T., Holzäpfel, F., Bryant, W., Köpp, F., Ferch, M., Tafferner, A., and Winckelmans, G., "Research towards a wake-vortex advisory system for optimal aircraft spacing," *C. R. Physique*, Vol. 6(4-5), 2005, pp. 501–523.

[3]Spalart, P., "Airplane trailing vortices," *Annual Review of Fluid Mechanics*, Vol. 30(1), 1998, pp. 107–138.

[4]Robins, R. and Delisi, D., "Potential hazard of aircraft wake vortices in ground effect with crosswind." *Journal of Aircraft*, Vol. 2, 1993, pp. 201–206.

[5]Türk, L., Coors, D., and Jacob, D., "Behavior of wake vortices near the ground over a large range of Reynolds numbers," *Aerospace Science and Technology*, Vol. 3(2), 1999, pp. 71–81.

[6]Holzäpfel, F. and Steen, M., "Aircraft Wake-Vortex Evolution in Ground Proximity: Analysis and Parameterization," *AIAA Journal*, Vol. 45, 2007, pp. 218–227.

[7]Harvey, J. and Perry, F., "Flowfield produced by trailing vortices in the vicinity of the ground," *AIAA Journal*, Vol. 9(8), 1971, pp. 1659–1660.

[8]Dufresne, L., Baumann, R., Gerz, T., Winckelmans, G., Moet, H., and Capart, "Large Eddy Simulation of Wake Vortex Flows at Very High Reynolds Numbers: A Comparison of Different Methodologies," Tech. rep., AWIATOR, D1.14-16, 2005.

[9]Spalart, P., Strelets, M., Travin, A., and Shur, M., "Modelling the Interaction of a Vortex Pair with the Ground," *Fluid Dynamics*, Vol. 36(6), 2001, pp. 899–908.

[10]Proctor, F. H., Hamilton, D. W., and Han, J., "Wake Vortex Transport and Decay in Ground Effect: Vortex Linking with the Ground," *AIAA, 2000-0757, 38th Aerospace Sciences Meeting & Exhibit, Reno*, 1 2000.

[11]Fabre, D., Jacquin, L., and Loof, A., "Optimal perturbations in a four-vortex aircraft wake in counter-rotating configuration," *Journal of Fluid Mechanics*, Vol. 451, 2002, pp. 319–328.

[12]Duponcheel, M., Lonfils, T., Bricteux, L., and Winckelmans, G., "Simulations of three-dimensional wake vortices in ground effest using a fourth-order incompressible code," *7th National Congress on Theoretical and Applied Mechanics, Mons*, 2006.

[13]Georges, L., Geuzaine, P., Duponchel, M., Bricteux, L., Lonfils, T., Winckelmans, G., and Giovannini, A., "Technical Report 3.1.1-3, LES of two-vortex system in ground effect with and without wind," Tech. rep., Université catholique de Louvain (UCL), Institut de Mécanique des Fluides de Toulouse(IMFT), 2005.

[14]Proctor, F. H. and Han, J., "Numerical Study of Wake Vortex Interaction with the Ground using the Terminal Area Simulation System," *AIAA, 99-0754, 37th Aerospace Sciences Meeting & Exhibit, Reno*, 1 1999.

[15]Manhart, M., "A Zonal Grid Algorithm for DNS of Turbulent Boundary Layer," *Computer and Fluids*, Vol. 33, No. 3, 2004, pp. 435–461.

[16]Meneveau, C., Lund, T. S., and Cabot, W. H., "A Lagrangian dynamic subgrid-scale model of turbulence," *Journal of Fluid Mechanics*, Vol. 319, 1996, pp. 353–385.

[17]Hokpunna, A. and Manhart, M., "Compact Fourth-order Finite Volume Method for Numerical Solutions of navier-Stokes Equations on Staggered Grids," *Journal of Computational Physics*, Vol. 229, No. 20, 2010, pp. 7545–7570.

[18]Brown, A. R., Hobson, J. M., and Wood, N., "Large-eddy simulation of neutral turbulent flow over rough sinusoidal ridges," *Boundary-Layer Meteorology*, Vol. 98, 2001, pp. 411–441.

[19]Schlichting, H. and Gersten, G., *Grenzschicht-Theorie*, Springer, 1997.

[20]Jimenez, J. and Moin, P., "The minimal flow unit in near-wall turbulence." *Journal of Fluid Mechanics*, Vol. 225, 1991, pp. 213–240.

[21]Grötzbach, G., "Direct numerical and large eddy suimulations of turbulent channel flows." *Encyclopedia of fluid mechanics (ed. N. Cheremisinoff)*., West Orange, NJ, 1987.

[22]Lamb, H., *Hydrodynamics*, Cambridge University Press, 1957.

[23]Saffman, P. G., "The approach of a vortex pair to a plane surface in inviscid fluid," *Journal of Fluid Mechanics*, Vol. 92(3), 1979, pp. 497–503.

[24]Doligalski, T. L., Smith, C., and A., W. J. D., "Vortex interactions with walls," *Annual Review of Fluid Mechanics*, Vol. 26, 1994, pp. 573–616.

[25]Holzäpfel, F., Gerz, T., Frech, M., Tafferner, A., Köpp, F., Smalikho, I., Rahm, S., Hahn, K.-U., and Schwarz, C., "The Wake Vortex Prediction and Monitoring System WSVBS - Part I: Design," *Air Traffic Control Quarterly*, Vol. 17, No. 4, 2009, pp. 301–322.

[26]Holzäpfel, F., "Probabilistic Two-Phase Wake Vortex Decay and Transport Model," *Journal of Aircraft*, Vol. 40, No. 2, 2003, pp. 323–331.

[27]Steen, M., *Analyse und Parametrisierung des Wirbelschleppenverhaltens in Bodennähe*, Master's thesis, Technische Universitaet Braunschweig, 2005.

[28]Holzäpfel, F., Gerz, T., and Baumann, R., "The Turbulent Decay of Trailing Vortex Pairs in Stably Stratified Environments," *Aerospace Science and Technology*, Vol. 5, No. 2, 2001, pp. 95–108.

[29]Misaka, T., Holzäpfel, F., Hennemann, I. Gerz, T., Manhart, M., and Schwertfirm, F., "Vortex bursting and tracer transport of a counter-rotating vortex pair," *Physics of Fluids*, Vol. 24, 2012, pp. (025104–1) – (025104–21).

[30]Holzäpfel, F., Hofbauer, T., Darracq, D., Moet, H., Garnier, F., and Ferreira Gago, C., "Analysis of wake vortex decay mechanisms in the atmosphere," *Aerospace Science and Technology*, Vol. 7, 2003, pp. 263–275.

[31]Cantwell, B., Coles, D., and Dimotakis, P., "Structure and entrainment in the place of symmetry of a turbulent spot." *Journal of Fluid Mechanics*, Vol. 87, 1978, pp. 641–672.

[32]Butler, K. M. and Farrell, B. F., "Optimal perturbations and streak spacing in turbulent shear flow." *Physics of Fluids*, Vol. 5, 1993, pp. 774–777.

[33]Ortega, J. M., Bristol, R. L., and Savas, Ö., "Experimental study of the instability of unequal strength counter-rotating vortex pairs." *Journal of Fluid Mechanics*, Vol. 474, 2003, pp. 35–84.

[34]Moet, H., Laporte, F., Chevalier, G., and Poinsot, T., "Wave propagation in vortices and vortex bursting," *Physics of Fluids*, Vol. 17, 2005, pp. 054109.